Reactions induced by 30 MeV ^{3}He beam on ^{9}Be : cluster transfer reactions*

B. A. Urazbekov[1,2,3] T. Issatayev[1,2,4†] S. M. Lukyanov[4] A. Azhibekov[2,4,5] A. S. Denikin[4,6] K. Mendibayev[2,4]
D. M. Janseitov[2,3,7] Yu E. Penionzhkevich[4] K. A. Kuterbekov[1] T. K. Zholdybayev[2,7]

[1]Gumiliyev Eurasian National University, 2 Satpayev Str,Astana, Kazakhstan
[2]Institute of Nuclear Physics, 1 Ibragimov Str, Almaty, Kazakhstan
[3]Bogolubov Laboratory of Theoretical Physics, JINR, 20 Joliot Curie Str, Dubna, Russia
[4]Flerov Laboratory of Nuclear Reactions, JINR, 20 Joliot Curie Str, Dubna, Russia
[5]Korkyt-ata State University, 29A Aiteke-Byi Str, Kyzylorda, Kazakhstan
[6]Dubna State University, 19 Universitetskaya Str, Dubna, Russia
[7]Al-Farabi Kazakh National University, Almaty, Kazakhstan

Abstract: An experiment was conducted for studying the cluster structure of ^{9}Be induced by ^{3}He ions at an energy of 30 MeV. As results of the nuclear reaction ^{3}He + ^{9}Be, the differential cross sections for the exit channels – elastic, inelastic, α + ^{8}Be, ^{6}He + ^{6}Be, ^{6}Li + ^{6}Li, and ^{7}Be + ^{5}He – were measured. Elastic and inelastic scattering data were treated within both the optical model and coupled channel method. A new set of optical potentials was considered for the elastic scattering. The deformation parameter $\delta_2$was established for the transition $3/2 \rightarrow 5/2$. Cluster transfer reactions were analyzed via the coupled reaction channel method. The nuclear reactions with the exit channels ^{6}He + ^{6}Be, ^{6}Li + ^{6}Li, and ^{7}Be + ^{5}He were complemented by two-step transfer mechanisms. The contribution of each reaction mechanism were shown and compared with the findings of other authors.

Keywords: cluster transfer, reaction mechanisms, coupled equations

DOI: 10.1088/1674-1137/ad0376

I. INTRODUCTION

In most cases of light nuclei, with $A<12$, the nucleons may form a group. The group in nuclear physics is often termed as the cluster. The relative motion of such structures determines general characteristics and properties. In this manner, analyzing the cluster structure of light nuclei has emerged as a primary task in nuclear physics, both in terms of theoretical studies and experimental investigations.

Nucleus ^{9}Be is an attractive nucleus due to its many internal properties. Specifically, experimental data points, such as the low binding energy of the p-shell neutron -1.66 MeV (*e.g.*, see [1]), large quadrupole moment of $+53.3\pm3$ mb [2, 3], and positive parity in the first excited state $\frac{1}{2}^{+}$ at 1.684 MeV (*e.g.*, see [1], indicate its unique structure. Therefore, in the cluster model framework, the nucleus can be supposed to have the configurations, such as $2\alpha+n$, α + ^{5}He, ^{8}Be + n, and others.

The cluster structure of ^{9}Be has been extensively studied within the various approaches [4–9]. In recent studies from Refs. [10, 11], the elastic scattering data of α-particles and of d on ^{9}Be have been treated within the cluster models α+ ^{5}He and ^{8}Be +n. The authors demonstrated, using the example of elastic scattering, that the interaction potentials of projectiles can be analyzed using the cluster folding model within various configurations such as α+ ^{5}He and ^{8}Be +n. Furthermore, at backward angles, the spectroscopic amplitudes have been determined through calculations of elastic transfer reactions.

It is interesting to note an analysis of the two-neutron transfer in the nuclear reactions induced by ^{7}Be radioactive beam on the target nucleus ^{9}Be [12]. The two-nucleon spectroscopic amplitudes were derived using the shell model framework and applied to the elastic transfer channel. The authors successfully accounted for the experimental data on excess cross sections using Coupled Reaction Channel (CRC) calculations that integrate both elastic scattering and elastic transfer mechanisms. This suggests that the nucleus ^{9}Be may also possess a cluster structure similar to ^{7}Be +$2n$.

In the study [13], the nuclear reactions resulting from ^{3}He + ^{9}Be at an energy of 63 MeV have been analyzed. The elastic channel as well as the exit channels ^{7}Be + ^{5}He, ^{6}Li + ^{6}Li were calculated within the CRC method. For these channels, all the possible transfer mechanisms

Received 15 August 2023; Accepted 17 October 2023; Published online 18 October 2023
* Supported by the Science Committee of the Ministry of Science and Higher Education of the Republic of Kazakhstan (AP14870958)
† E-mail: issatayev@jinr.ru

were supposed. In particular, the two-step transfer mechanisms beginning with n pick-up effectively enhances the underestimated cross sections for the channels ^{7}Be + ^{5}He and ^{6}Li + ^{6}Li. It shows that the p-shell neutron is loosely bound, and, in turn, the nucleus ^{9}Be has the cluster structure ^{8}Be+n.

The same experimental study with nuclear reaction ^{3}He + ^{9}Be was performed, but at the laboratory energy of 30 MeV [14]. Pure optical model and DWBA calculations performed in this study require more sophisticated theoretical models. Therefore, our aim is to analyze the experimental data [14] within the cluster model of ^{9}Be and to probe all possible transfer mechanisms. We focus on the internal structure of ^{9}Be, presenting fresh data missing in Refs. [14, 15], and on the data in more accurate processed form.

This paper is organized as follows. The first section offers detailed information about the experimental methodology. The second section focuses on both elastic and inelastic scattering. A discussion of the cluster transfer channels is presented in the subsequent section. Finally, the main findings and conclusions are summarized.

II. EXPERIMENTAL PROCEDURE

The experiment on the nuclear reaction ^{3}He and ^{9}Be at a laboratory energy of 30 MeV was conducted at the Nuclear Physics Institute (NPI), Řež, Czech Republic. During the course of the experiment, an average beam current was maintained at 10 enA. The self-supporting ^{9}Be target with a thickness of 11 μm was developed with a foil, which was highly purified up to 99%. The resonances of the contamination by the carbon and oxygen isotopes were not detected in the energy spectra.

Particle identification was based on the ΔE-E method, *i.e.* measurements of the energy-loss ΔE and residual energy E_r. Four Si-Si(Li) telescopes consisting of detectors ΔE_0, ΔE, and E_r were mounted to register scattered ions with the thicknesses of 10 μm, 100 μm, and 3 mm, respectively. The acceptance angle of each telescope was $\sim 0.6^{\circ}$ in the scattering plane, and their solid angle was ~ 0.2 msr. The good energy resolutions of both ΔE and E_r detectors provided unambiguous identification of A and Z of each product. The over-all energy resolution was 150 – 200 keV.

The excitation energy spectra for ^{9}Be, ^{6}Be, ^{6}Li, and ^{5}He are shown in Fig. 1. The ground and excited states of the nuclei ^{9}Be, ^{6}Be, ^{6}Li, and ^{5}He were identified in the following reaction channels: ^{9}Be (^{3}He, ^{3}He) ^{9}Be (see panel *a*), ^{9}Be (^{3}He, ^{6}He) ^{6}Be (*b*), ^{9}Be (^{3}He, ^{6}Li) ^{6}Li (*c*), and ^{9}Be (^{3}He, ^{7}Be) ^{5}He (*d*). The energy calibration of ΔEs and E_r detectors was performed considering well-known states, which are strongly excited in the spectra. The calibration appeared to be practically linear. This allows us to determine the positions of all excited states in the spectra. The total energies were calculated as the sum over the calibrated energy losses ΔE_s and the residual energy E_r. The excitation energy spectra were constructed as $E_{g.s}$ (position) - E_{total}.

The peaks were identified using a fitting procedure that employs standard Gaussian decomposition. Utilizing the established energy calibration, the positions and widths of the peaks were fixed in line with widely recognized experimental data. It is important to note that the width of each state in the spectrum may encompass several factors: the natural width, apparatus width of the set-up, and energy spread. The latter is caused by the emitting particles, which may originate either at the beginning or at the end of the target foil. Additionally, the background areas are delineated in Fig. 1. They are mainly due to the phase volumes which depend on the threshold energy in the following break-up processes:

- ^{9}Be $\rightarrow$^{8}Be + n (see Fig. 1, panel *a*, red dashed curve) or ^{4}He + ^{5}He (*a*, blue dot-dashed);
- ^{6}Be $\rightarrow$^{4}He + 2p (*b*, red dashed) or ^{5}Li + p (*b*, blue dot-dashed);
- ^{6}Li $\rightarrow$ ^{4}He+ d (*c*, red dot-dashed) or ^{4}He + p + n (*c*, blue dashed);
- ^{5}He $\rightarrow$ ^{4}He+ n (*d*, red dashed).

The absolute error in measuring the cross section is confined to no more than 15%. This error predominantly arises from several factors: inaccuracies in peak decomposition, statistical errors in the count of events in the subtracted peak, errors in determining the target's thickness, inaccuracies in solid angle values, event losses, and errors in current measurement.

III. ELASTIC AND INELASTIC CHANNELS

Elastic scattering

The differential cross section of the elastic scattering of ^{3}He from the nucleus ^{9}Be was treated within the optical model framework. Numerical calculations were conducted by means of the FRESCO code [16]. The optical potential used in the OM calculations was considered in the form:

$$U(R) = -V(R) - \mathrm{i}W(R) + V^{SO}(R)(\mathbf{l}\cdot\sigma) + V^{C}(R), \qquad (1)$$

where R denotes the distance between ^{3}He and ^{9}Be, and V^{V}, W^{V} denote the real and imaginary volume potential terms, and V^{SO} and V^{C} denote the spin-orbit and Coulomb potentials. The volume potentials may represent the Woods-Saxon (WS) potential [17]:

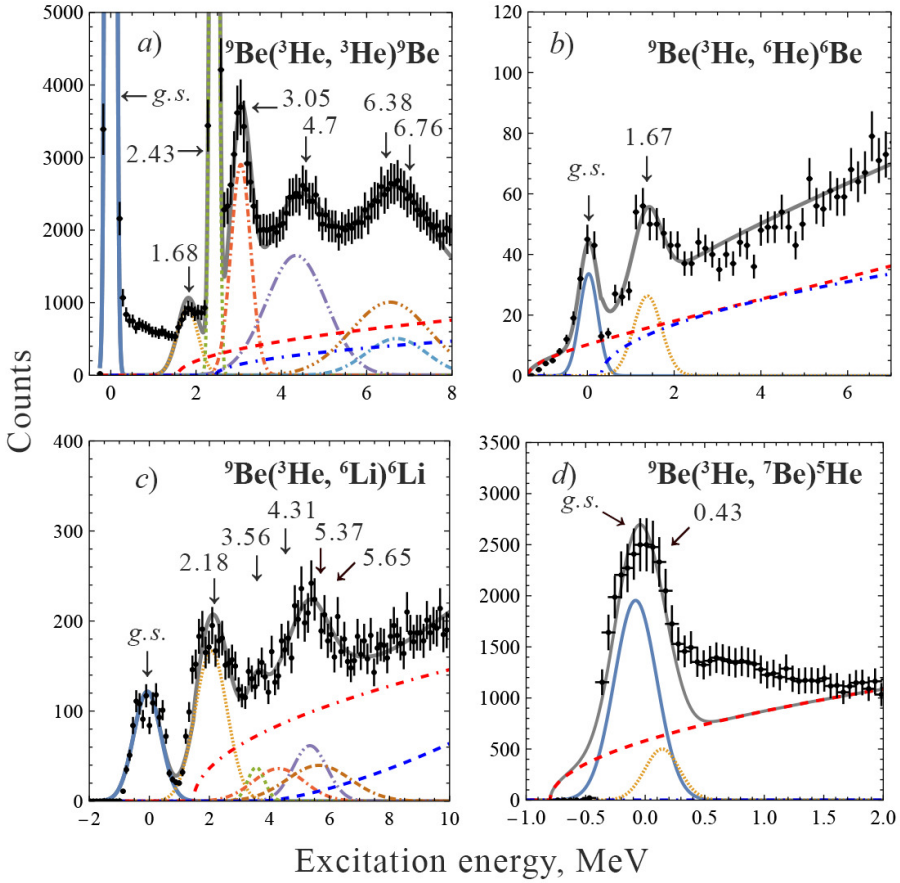

Fig. 1. (color online) Excitation energy spectra of ^{9}Be (a), ^{6}Be (b), ^{6}Li (c), and ^{5}He (d) for the nuclear reaction ^{3}He +^{9}Be at $E_{\rm lab}$ = 30 MeV measured at $\theta_{\rm lab}$ = 12°. The total fit for each spectrum and subtracted peaks are shown. The background was fitted considering the three-body and four-body breakup processes (For more information, please refer to the text).

$$V(R) = V_0^V f_{R_V,a_V}(R), \quad f_{R_0,a_0}(R) = \left[1+\exp\left(\frac{R-R_0}{a_0}\right)\right]^{-1}, \tag{2}$$

where V_0 denotes the depth of the potential, r_0 denotes the average distance, and a_0 denotes the diffusion parameter. The spin-orbit term can be expressed in the following form:

$$V^{SO}(R) = V_0^{SO}\left(\frac{\hbar}{m_\pi c}\right)^2 \frac{1}{R}\frac{\rm d}{{\rm d}R} f_{R_{SO},a_{SO}}(R), \tag{3}$$

while the Coulomb term was considered as the interaction of a point-charge with a uniformly charged sphere as follows:

$$V^C(R) = \begin{cases} \dfrac{Z_1 Z_2 {\rm e}^2}{2R_C}\left(3-\dfrac{R^2}{R_C^2}\right), & \text{for } R \le R_C, \\ \dfrac{Z_1 Z_2 {\rm e}^2}{R}, & \text{for } R > R_C. \end{cases} \tag{4}$$

As a staring point for the seeking optical potential, we considered global optical parameters from Ref. [18]. The elastic scattering cross section was fitted on the measured experimental data. It was performed via`SFRESCO` [16]. The obtained potential parameters are listed in Table 1.

Given that the spin reorientation is not forbidden, e.g. $3/2 \to 3/2$ or $5/2 \to 5/2$, it was also considered in the CC calculations. The calculated CC results are presented in Fig. 2. Specifically, OM and CC calculations are almost identical. Explicit consideration of the coupling between the inelastic channel and the spin reorientation leads to modifications in the optical potential. Hence, the real part of the optical potential becomes deeper, whereas the depth of the imaginary part decreases (see mOP, Table 1).

The role of the inelastic channel, $5/2 \to 3/2$, in the elastic channel turned out to be non-negligible. The effect of spin reorientation is one magnitude lower than the OM estimation. The extrema point of SR coincides with the extrema of mOP. This feature is a typical characteristic of spin reorientation effects. A similar pattern was also reported in Ref. [13].

Inelastic scattering

The differential cross sections for the inelastic scatter-

Table 1. Potential parameters used in the optical model and CRC calculations.

	V_0/MeV	$r_V^{a)}$/fm	a_V/fm	W_0/MeV	$r_W^{a)}$/fm	a_W/fm	V_i/MeV	$r_i^{a)}$/fm	a_i/fm	$r_C^{a)}$/fm
^{3}He + ^{9}Be	101.9	0.700	0.777	30.81	0.854	0.817	2.5[c)]	0.708	0.720	0.767
	103.9[b)]			23.81[b)]						
^{7}Be + ^{5}He	258.516	0.588	0.726	18.0	0.773	0.6	45.4[d)]	0.566	0.843	0.734
^{6}Li + ^{6}Li	114.0	0.64	0.859	45.6	0.831	0.807				0.649
^{7}Li + ^{5}Li	114.0	0.606	0.853	38.448	0.82	0.809				0.588
α + ^{8}Be	121.0	0.252	1.01	17.0	1.38	0.34				0.724

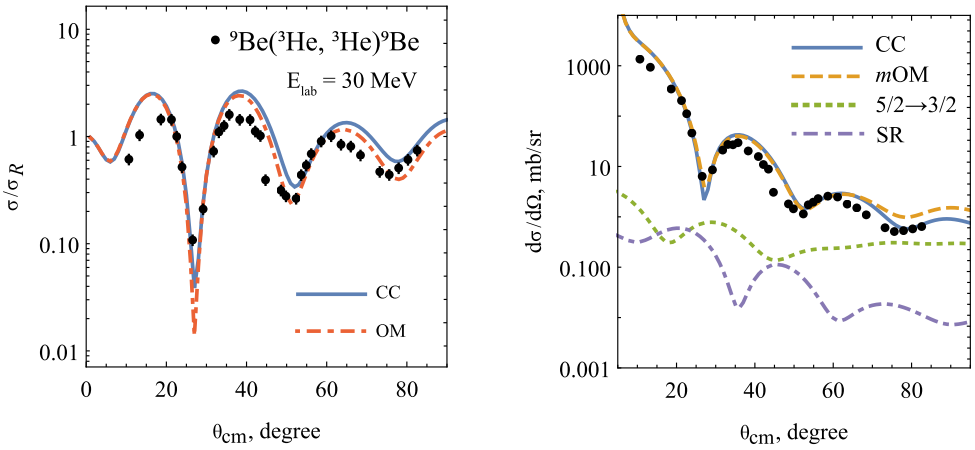

Fig. 2. (color online) Theoretical cross sections for the elastic scattering ^{9}Be(^{3}He,^{3}He)^{9}Be in comparison with measured cross section data at E_{lab} =30 MeV. Left panel: Calculated cross sections are provided in ratio to the Rutherford scattering and conducted within the coupled channels (CC, χ^2 = 28.3) and optical model (OM, χ^2 = 14.85) methods. Right panel: the same CC cross section in absolute unit, but presented in terms of the optical model cross section with modified potential parameters (mOM), the contribution of inelastic channel (5/2 → 3/2) and the spin re-orientation effect (SR).

ing of ^{3}He on ^{9}Be with the excitation 2.43 MeV is calculated in the framework of coupled channels (CC) method [16]. For the CC calculations, the mOP potential was used.

To explicitly track the couplings, we opted not to use a rotational model but instead employed a more general approach. In this scenario, the strength of the coupling factor is determined by:

$$RDEF(\lambda, J \to J') = (-1)^{J+J'+|J-J'|}\sqrt{2J+1}\langle JK\lambda 0|J'K\rangle\delta_\lambda^{J\to J'} \tag{5}$$

where J and J' denote the spins of initial and final states, and K denotes the projection. The deformation length may have the following form:

$$\delta_\lambda^{J\to J'} = \beta_\lambda^{J\to J'} R_i. \tag{6}$$

Here, $\beta_\lambda^{J\to J'}$ denotes the deformation parameters, and R_i denotes the interaction radius.

The calculated differential cross sections for the inelastic scattering channel with ^{9}Be excitation at 2.43 MeV are shown in Fig. 3. The spin re-orientation, *i.e.*, the transition $\frac{5}{2} \to \frac{5}{2}$, has also been implemented in the coupling scheme.

The calculated cross section for the excitation process initially falls short of matching the experimental data. Nevertheless, when the spin re-orientation effect is factored in, it boosts the cross section, aligning the combined results closely with the experimental observations. However, an exception occurs in the cross section data starting from 65 degrees, likely attributable to the influences of other excitation modes not explicitly incorporated in the CC calculation.

In this study, the best agreement of theoretical analyses with data is obtained if one uses the deformation length $\delta_2^{3/2\to 5/2}$ =1.97 fm. In the study dedicated to the scattering of α-particles on ^{9}Be in Ref. [19], the length is 1.61 fm. On the contrary, deformation length of 2.63 fm is obtained in Ref. [20] in reactions p + ^{9}Be. Our results on the deformation length occupy an intermediate position when compared to values presented in other sources. Generally, the structure of ^{9}Be should not be influenced

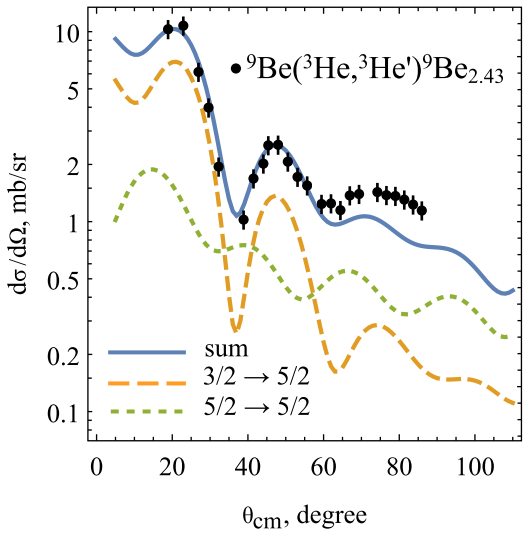

Fig. 3. (color online) Inelastic scattering data in comparison with the CC calculation results in terms of different coupling contributions: the transition from $\frac{3}{2}^{-}$ to $\frac{5}{2}^{-}$ states (dashed) and spin re-orientation for state $\frac{5}{2}^{-}$ (doted).

by the dynamics of nuclear reactions. However, this variance can be attributed to the distinct nature of the interactions between the projectiles and the protons and neutrons in the target nucleus [21]. Consequently, the deformation lengths derived directly from inelastic scattering caused by various projectiles may also differ.

In terms of the Eq. (6), the values of the deformation parameters vary due to the ambiguity in the interaction radius. If the radius parameter of the optical potential mOP is considered as $r = 0.7$ fm, the deformation parameter corresponds to 0.8. This reproduces the results of the previous study in Ref. [22] with the same experimental data and applied theoretical method.

IV. CLUSTER-TRANSFER REACTIONS

A. ^{7}Be + ^{5}He channel

In this study, reaction ^{9}Be (^{3}He, ^{7}Be) ^{5}He is supposed to have both one-step and two-step transfer mechanisms, which are demonstrated schematically in Fig. 4. The one-step mechanism occurs by transferring α-particles, while the two-step mechanisms may have n- ^{3}He, ^{3}He -n, d-d. Moreover, we find that the transfer of $2n$ cluster is also possible at the backward angles of scattering. Therefore, the CRC calculation covers all mentioned transfer mechanisms, and the resulting differential cross section for the reaction ^{9}Be (^{3}He, ^{7}Be) ^{5}He is represented as

$$\frac{\mathrm{d}\sigma(\theta)}{\mathrm{d}\Omega} = \frac{1}{(2J_a+1)(2J_A+1)} |f_{\mathrm{I}}(\theta) + f_{\mathrm{II}}(\theta)|^2, \qquad (7)$$

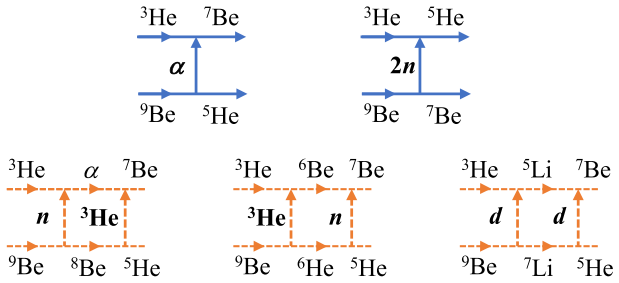

Fig. 4. (color online) Reaction schemes for transfer mechanisms in ^{9}Be (^{3}He, ^{7}Be) ^{5}He : one-step (solid) and two-step (dashed) mechanisms.

where the amplitudes of the one-step $f_{\mathrm{I}}(\theta)$ and two-step $f_{\mathrm{II}}(\theta)$ transfer mechanisms are as follows:

$$f_{\mathrm{I}}(\theta) = f_{\alpha}(\theta) + f_{2n}(\theta - \pi),$$
$$f_{\mathrm{II}}(\theta) = f_{n-^{3}\mathrm{He}}(\theta) + f_{^{3}\mathrm{He}-n}(\theta) + f_{d-d}(\theta). \qquad (8)$$

The optical potential mOP is selected as the potential for the entrance channel. For the exit channels, we utilized an optical potential with the global optical parameters from Ref. [23].

The optical potential of the intermediate channel α + ^{8}Be has been preferred to a potential, which reproduces the experimental cross sections of ^{9}Be (^{3}He, α) ^{8}Be in the exit channel. The bound state wave functions have been built on the Woods-Saxon shaped potential, with the depths fitted on the binding energies. However, the resonance states were considerd as the quasi-bound states, *i.e.* taken by means of the same procedure, but with the binding energy of 0.01 MeV. Spectroscopic amplitudes were considered from Refs. [12, 13, 24] and presented in Table 2.

All CRC calculations have been performed using the FRESCO code [16]. The two-step transfer reactions have been calculated using the N-step DWBA iteration neglecting the back couplings. The prior and post modes were used for the first and second couplings, respectively, aimed at avoiding the non-orthogonality term. The results of the CRC calculations are shown in Fig. 5. The optical potentials used in these calculations are given in Table 1.

The direct transfer of the α-particle obviously prevails on other transfer mechanisms (see Fig. 5, *left panel*). It is interesting to note the different contribution of the transfer of system n + ^{3}He. It turns out that system n + ^{3}He easily transfers in the way of n- ^{3}He rather that ^{3}He -n. The reason for this may lie in the p-shell valence neutron, which is loosely bound to ^{9}Be. Next contributor to the cross section is $2n$ transfer at the backward scattering angles. Starting from 60°, it provides only α-transfer. However, starting from 90°, the transfer mechanism $2n$ may stand as a main contributor. To validate this hypo-

Table 2. Spectroscopic data used in the CRC calculations for Composite (A) comprising Core (C) and Valence particle (v) with configuration nlj. Most of spectroscopic amplitudes (SA) were obtained from Refs. [12, 13, 24].

A		C		v		nlj	SA	A		C		v		nlj	SA
^{6}Li	1	^{3}He	0.5	t	0.5	$2S_{0.5}$	−0.943	^{9}Be	1.5	^{5}He	1.5	α	0	$2D_{2}$	−0.530
^{6}Li	3	^{3}He	0.5	t	0.5	$1D_{2.5}$	−0.943	^{7}Be	1.5	^{6}Li	1_{1}	p	0.5	$1P_{0.5}$	−0.657
^{6}Li	1	^{3}He	0.5	t	0.5	$1D_{1.5}$	0.943	^{7}Be	1.5	^{6}Li	3	p	0.5	$1P_{1.5}$	0.738
^{9}Be	1.5	^{6}Li	1_{1}	t	0.5	$2P_{0.5}$	−0.192	^{7}Be	1.5	^{6}Li	1_{2}	p	0.5	$1P_{0.5}$	0.147
^{9}Be	1.5	^{6}Li	1_{1}	t	0.5	$2P_{1.5}$	−0.215	^{7}Be	1.5	^{6}Li	1_{2}	p	0.5	$1P_{1.5}$	−0.132
^{9}Be	1.5	^{6}Li	3	t	0.5	$2P_{1.5}$	−0.594	^{7}Be	1.5	^{6}Li	1_{1}	p	0.5	$1P_{1.5}$	−0.735
^{9}Be	1.5	^{6}Li	3	t	0.5	$1F_{3.5}$	−0.316	^{6}Li	1_{1}	^{5}He	1.5	p	0.5	$1P_{0.5}$	−0.596
^{9}Be	1.5	^{6}Li	1_{2}	t	0.5	$2P_{0.5}$	−0.118	^{6}Li	1_{1}	^{5}He	1.5	p	0.5	$1P_{1.5}$	0.667
^{9}Be	1.5	^{6}Li	1_{2}	t	0.5	$1F_{2.5}$	−0.324	^{6}Li	3	^{5}He	1.5	p	0.5	$1P_{1.5}$	0.500
^{4}He	0	^{3}He	0.5	n	0.5	$1S_{0.5}$	−0.741	^{6}Li	1_{2}	^{5}He	1.5	p	0.5	$1P_{0.5}$	0.333
^{9}Be	1.5	^{8}Be	0	n	0.5	$1P_{1.5}$	0.791	^{6}Li	1_{2}	^{5}He	1.5	p	0.5	$1P_{1.5}$	0.298
^{9}Be	2.5	^{8}Be	0	n	0.5	$1P_{1.5}$	−0.816	^{5}Li	1.5	^{3}He	0.5	d	1	$1P_{1}$	0.456
^{9}Be	2.5	^{8}Be	2	n	0.5	$1P_{1.5}$	−0.986	^{5}Li	1.5	^{3}He	0.5	d	1	$1P_{2}$	1.021
^{9}Be	2.5	^{8}Be	0	n	0.5	$1P_{0.5}$	0.242	^{9}Be	1.5	^{7}Li	1.5	d	1	$2S_{1}$	−0.226
^{9}Be	2.5	^{8}Be	2	n	0.5	$1P_{0.5}$	0.417	^{9}Be	1.5	^{7}Li	1.5	d	1	$1D_{1}$	0.111
^{6}Li	1.0	^{4}He	0	d	1.0	$2S_{1}$	1.061	^{9}Be	1.5	^{7}Li	1.5	d	1	$1D_{3}$	−0.624
^{6}Li	3.0	^{4}He	0	d	1.0	$1D_{3}$	1.061	^{6}Li	1_{1}	^{5}Li	1.5	n	0.5	$1P_{0.5}$	0.597
^{8}Be	0	^{6}Li	1_{1}	d	1.0	$2S_{1}$	1.146	^{6}Li	1_{1}	^{5}Li	1.5	n	0.5	$1P_{1.5}$	−0.667
^{8}Be	0	^{6}Li	1_{1}	d	1.0	$1D_{1}$	0.112	^{6}Li	3	^{5}Li	1.5	n	0.5	$1P_{1.5}$	1.095
^{8}Be	0	^{6}Li	3	d	1.0	$2S_{1}$	0.089	^{6}Li	1_{2}	^{5}Li	1.5	n	0.5	$1P_{0.5}$	−0.333
^{8}Be	0	^{6}Li	3	d	1.0	$1D_{1}$	0.414	^{6}Li	1_{2}	^{5}Li	1.5	n	0.5	$1P_{1.5}$	−0.298
^{8}Be	0	^{6}Li	3	d	1.0	$1D_{2}$	−0.477	^{7}Li	1.5	^{6}Li	1_{1}	n	0.5	$1P_{0.5}$	−0.657
^{8}Be	0	^{6}Li	3	d	1.0	$1D_{3}$	0.744	^{7}Li	1.5	^{6}Li	1_{1}	n	0.5	$1P_{1.5}$	−0.735
^{8}Be	0	^{6}Li	3	d	1.0	$2S_{1}$	0.850	^{7}Li	1.5	^{6}Li	3	n	0.5	$1P_{1.5}$	0.738
^{8}Be	2	^{6}Li	3	d	1.0	$2S_{1}$	0.747	^{7}Li	1.5	^{6}Li	1_{2}	n	0.5	$1P_{0.5}$	0.147
^{8}Be	2	^{6}Li	3	d	1.0	$1D_{1}$	0.079	^{7}Li	1.5	^{6}Li	1_{2}	n	0.5	$1P_{1.5}$	−0.132
^{8}Be	2	^{6}Li	3	d	1.0	$1D_{2}$	0.259	^{6}He	0	^{5}He	1.5	n	0.5	$1P_{1.5}$	−0.867
^{8}Be	2	^{6}Li	3	d	1.0	$1D_{3}$	0.538	^{7}Be	1.5	^{6}Be	0	n	0.5	$1P_{1.5}$	−0.935
^{8}Be	0	^{6}Li	1_{2}	d	1.0	$2S_{1}$	−0.237	^{6}He	0	^{4}He	0	$2n$	1.0	$1S_{0}$	0.909
^{8}Be	0	^{6}Li	1_{2}	d	1.0	$1D_{1}$	0.372	^{8}Be	0	^{6}Be	0	d	1.0	$1S_{0}$	−1.200
^{8}Be	2	^{6}Li	1_{2}	d	1.0	$2S_{1}$	0.371	^{7}Be	1.5	^{4}He	0	^{3}He	0.5	$2P_{1.5}$	−1.091
^{8}Be	2	^{6}Li	1_{2}	d	1.0	$1D_{1}$	0.053	^{8}Be	0	^{5}He	1.5	^{3}He	0.5	$2P_{1.5}$	−1.102
^{8}Be	2	^{6}Li	1_{2}	d	1.0	$1D_{2}$	−0.356	^{6}Be	0	^{3}He	0.5	^{3}He	0.5	$2S_{0.5}$	0.943
^{8}Be	2	^{6}Li	1_{2}	d	1.0	$1D_{3}$	−0.130	^{9}Be	1.5	^{6}He	0	^{3}He	0.5	$2P_{1.5}$	−0.215
^{5}He	1.5	^{3}He	0.5	$2n$	0	$1P_{1}$	−0.913	^{7}Be	1.5	^{6}Be	0	n	0.5	$1P_{0.5}$	−1.091
^{9}Be	1.5	^{7}Be	1.5	$2n$	0	$2S_{0}$	0.247	^{6}He	0	^{5}He	1.5	n	0.5	$1P_{1.5}$	−1.102
^{9}Be	1.5	^{7}Be	1.5	$2n$	0	$2D_{2}$	0.430	^{7}Be	1.5	^{5}Li	1.5	d	1	$2S_{1}$	−0.647
^{6}Li	1_{1}	^{5}He	1.5	p	0.5	$1P_{0.5}$	−0.597	^{7}Be	1.5	^{5}Li	1.5	d	1	$1D_{1}$	−0.121
^{6}Li	1_{1}	^{5}He	1.5	p	0.5	$1P_{1.5}$	0.667	^{7}Be	1.5	^{5}Li	1.5	d	1	$1D_{3}$	0.647
^{7}Be	1.5	^{6}Li	1_{1}	p	0.5	$1P_{0.5}$	−0.657	^{7}Li	1.5	^{5}He	1.5	d	1	$1D_{3}$	0.647
^{7}Be	1.5	^{6}Li	1_{1}	p	0.5	$1P_{1.5}$	−0.735	^{7}Li	1.5	^{5}He	1.5	d	1	$2S_{1}$	−0.647
^{7}Be	1.5	^{6}Li	2	p	0.5	$1P_{1.5}$	−1.095	^{7}Li	1.5	^{5}He	1.5	d	1	$1D_{1}$	−0.121
^{7}Be	1.5	^{6}Li	1_{2}	p	0.5	$1P_{1.5}$	−0.632	^{7}Li	1.5	^{5}He	1.5	d	1	$1D_{3}$	0.647
^{7}Be	1.5	^{6}Li	1_{2}	p	0.5	$1P_{0.5}$	−0.632	^{7}Be	1.5	^{3}He	0.5	α	0	$2P_{1}$	−0.950
^{7}Be	1.5	^{3}He	0.5	α	0	$2P_{1}$	1.091	^{9}Be	1.5	^{5}He	1.5	α	0	$3S_{0}$	−0.810
^{9}Be	1.5	^{5}He	1.5	α	0	$3S_{0}$	−0.810	^{9}Be	1.5	^{5}He	1.5	α	0	$2D_{2}$	−0.536

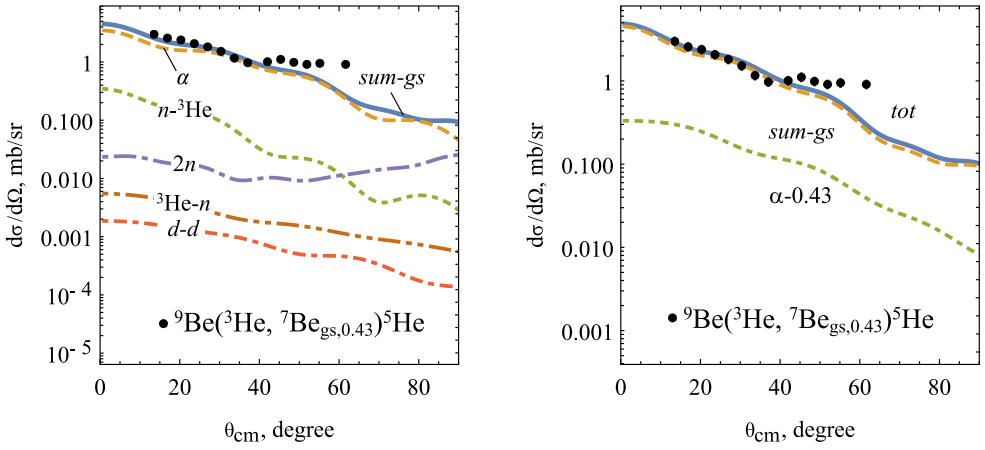

Fig. 5. (color online) Calculated CRC cross sections with the experimental data for the nuclear reaction ^{9}Be (^{3}He, ^{7}Be$_{gs,\ 0.43}$) ^{5}He. Cross sections are shown in terms of each considered transfer mechanism to the ground state of ^{7}Be (left panel). The incoherent sum of cross sections over the ground and first excited 0.43 states of ^{7}Be are also shown (right panel).

thesis, experiments need to be conducted at energies significantly higher than those used in the current study, namely above 30 MeV. Such higher energies would facilitate the identification of particles registered in the rear hemisphere. In similar experimental studies [12, 13] the 2*n* cluster transfer from ^{9}Be was also explored. In particular, the transfer of 2*n* cluster was observed by Umbelino *et al.* [12] in the elastic transfer reactions ^{7}Be + ^{9}Be. The transfer mechanism *d*-*d* has the lowest contribution among all of the proposed transfer mechanisms.

As a consequence of low detector resolution, we could not differentiate the registered ^{7}Be at the ground and first excited states. Nevertheless, we estimated its weight to the cross section via CRC calculations. It turns out that the cross section to the first excited state impacts less notably than the transfer mechanism *n*- ^{3}He (see Fig. 5, *right panel*). The calculated CRC cross sections effectively reproduce experimental data, with the exception of the last few points that have not been described with the proposed model.

B. ^{6}Li + ^{6}Li channel

The transfer mechanisms of cluster *t* is suggested to exhibit two-step processes as well, as it was suggested in Ref. [13]. The direct transfer *t*, and two-step transfer mechanisms of cluster *t* (see Fig. 6): *n*-*d*, *α*-*p*, 2*n*-*p*, and *d*-*n* were included in the CRC calculations. Differential cross sections for these transfer mechanisms are obtained analogously as in Eq. (8).

CRC calculations for the transfer of the cluster *t* utilized the WS optical potential for the entrance channel, and a WS shaped potential for the exit channel ^{6}Li + ^{6}Li. The potential parameters of the exit channel were determined by fitting to the experimental data on the elastic scattering of ^{6}Li + ^{6}Li at an energy of 40 MeV [25]. The obtained optical potential is shown in Table 1.

Apart from the fact that ^{6}Li was detected at the ground state, there were also two registered resonances. In the CRC calculations, they were considered through the coupling with the ground state of ^{6}Li.

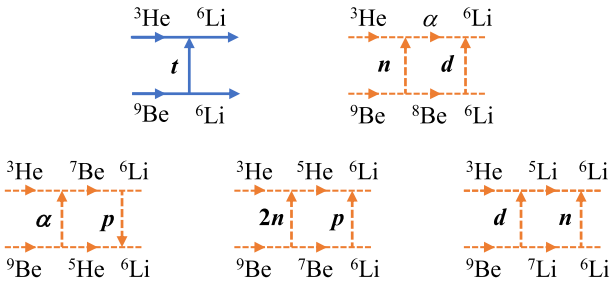

Fig. 6. (color online) Same as the caption of Fig. 4but for the reaction ^{9}Be (^{3}He, ^{6}Li) ^{6}Li.

The calculated differential cross sections for the channel ^{6}Li + ^{6}Li at the ground state are presented in Fig. 7 (*left panel*) with the contributions of each transfer mechanisms. The direct transfer of the cluster *t* dominates at the whole range of angles. The two-step transfer mechanism *n*-*d* is turns out to be less contributor than the transfer mechanism *t* in contrary to the studies by Rudchik *et al.* [13] within the same reaction, however, at the laboratory energy of 63 MeV. In the work the role of the transfer mechanism, *n*-*d* prevails over other processes including the direct transfer *t*. The cross section of the mechanism *n*-*d* has an oscillatory character, and it competes with the mechanism *α*-*p*. The latter transfer mechanisms, *i.e.* 2*n*-*p* and *d*-*n*, are insignificantly involved to the reaction.

Contribution order changes when ^{6}Li is excited (see Fig. 7, *right panel*). The transfer mechanism *t* remains unchanged, while *α*-*p* corresponds to the next contributor. Weakening of the mechanism *n*-*d* can be interpreted as the switching value in the spectroscopic amplitudes. In particular, the amplitude for the overlap $\langle ^{6}\mathrm{Li}_{2.19}|^{8}\mathrm{Be}\rangle$ with the configuration $2S_1$ is changed to 0.089. This type of a

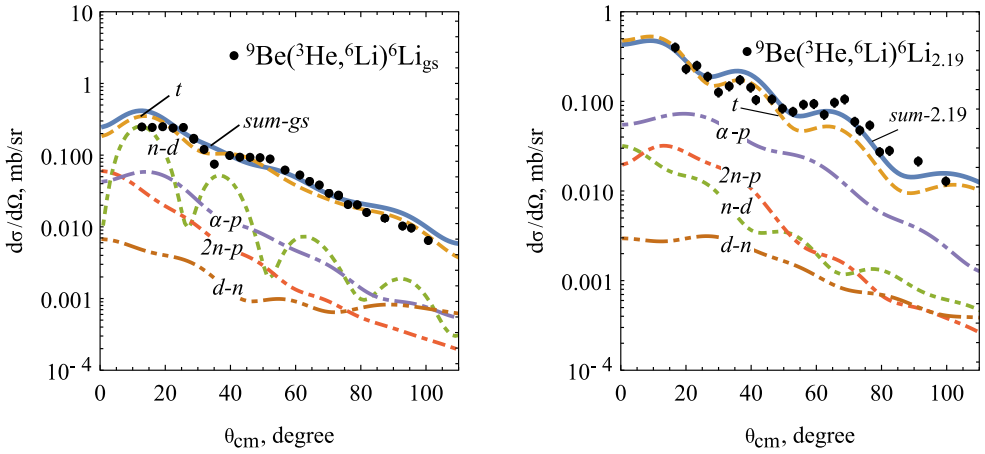

Fig. 7. (color online) Experimental data for nuclear reaction ^{9}Be(^{3}He, ^{6}Li)^{6}Li$_{gs}$ (left panel) and ^{9}Be(^{3}He, ^{6}Li)^{6}Li$_{2.19}$ (right panel) when compared to the calculated CRC cross sections in terms of channel contributions (please refer to the text for more details).

small spectroscopic amplitude would likely result in the *n-d* transfer mechanism being significantly less prevalent than the *d-n* mechanism. However, the spectroscopic amplitudes with $1D_{1,2,3}$ have non-negligible values, 0.414, −0.477, and 0.744, that do not allow *n-d* to disappear in the reaction.

Two resonances at 5.37 MeV and 5.65 MeV are mixed in the differential cross sections due to the experimental limitations. Therefore, we have included two channels into the CRC calculations. Calculation results for ^{9}Be (^{3}He, ^{6}Li) ^{6}Li * with an excitation of 5.65 MeV are demonstrated in Fig. 8 (*left panel*) in comparing with experimental data. The reaction mainly occurs through the direct transfer of cluster *t*. Two transfer mechanisms, 2*n-p* and *α-p*, affect nuclear reaction only up to 30°. Other transfer mechanisms, *i.e.*, *n-d* and *d-n*, almost do not influence the reaction.

Given that the transfer of cluster *t* has been the leading contributor in the ^{6}Li + ^{6}Li channel, the channel with an excitation of 5.37 MeV is calculated only with the transfer of *t*. The differential cross section of the channel with the 5.37 MeV excited state added incoherently with the channel at 5.65 MeV. Total cross section resulting from the CRC calculations are shown in Fig. 8 (*right panel*). The channel ^{6}Li+^{6}Li*, with the excitation of 5.37 MeV, contributes less than the channel at 5.65 MeV. The calculated differential cross sections effectively reproduce experimental data.

C. ^{6}He + ^{6}Be channel

The channel ^{6}He + ^{6}Be is a unique channel, as the transfer of system 3*n* is observed at the forward angles of scattering. In his case, we suggest three mechanisms of transfer (see Fig. 9, *left panel*): the two-step *n*-2*n* and 2*n*-*n*, and the one-step transfer of the cluster ^{3}He at the back hemisphere. Differential cross sections are obtained as well as they are expressed in Eq. (8). The results of the CRC calculations, detailing cross sections in terms of contributions from each of the three followed mechanisms, are illustrated in Fig. 9 (*right panel*).

The two-step transfer mechanisms, *i.e.* *n*-2*n* and 2*n*-*n*, compete with each other to provide almost smooth cross section. Starting from 60°, the most contribution is due to the transfer of ^{3}He. The CRC calculations are in good agreement with the experimental data.

However, CRC calculations for the channel ^{6}He + ^{6}Be were performed using large valued spectroscopic amplitudes. For example, the overlaps $\langle ^6\text{He}\,|\alpha\rangle$, $\langle ^6\text{Be}\,|\,^8\text{Be}\,\rangle$ exhibit the amplitudes ∼1.2. On the contrary, previous studies [26, 27] reported the amplitude for $\langle ^6\text{He}\,|\alpha\rangle$ equals ∼1.0. This type of difference between spectroscopic amplitudes indicates that there may be other processes not included in the reaction model. It is plausible that a one-step transfer of the *3n* system may occur in the ^{6}He + ^{6}Be channel. However, this issue is a distinct subject for investigation and cannot be precisely resolved using the model presented in this study. To obtain more accurate results, employing the four body problem approach might be beneficial.

V. CONCLUSION

Nuclear reactions involving ^{9}Be induced by ^{3}He at 30 MeV were investigated. The elastic channel was analyzed using the optical model, while the inelastic channel was examined through the CC approach. New parameters for the optical potential of the ^{3}He + ^{9}Be system at 30 MeV were derived. Employing this optical potential, the deformation parameter $\delta_2^{3/2\to5/2} = 0.8$ was extracted within the CC method, which could reproduce the results from another source [22].

In the cluster transfer channels, namely ^{7}Be + ^{5}He, ^{6}Li + ^{6}Li, and ^{6}He + ^{6}Be, all conceivable transfer mechanisms were considered. The differential cross sections for

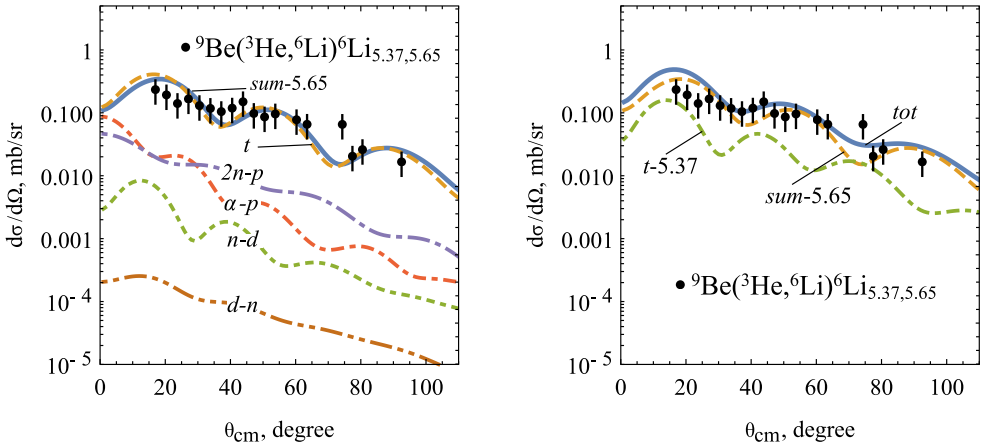

Fig. 8. (color online) Experimental data for nuclear reaction ^{9}Be (^{3}He, ^{6}Li) ^{6}Li $_{5.37,5.65}$ when compared to the CRC calculation results. The CRC cross section for the target-like nucleus ^{6}Li* at 5.65 MeV with the channel contributions (left panel). Total cross section summed incoherently over 5.65 MeV and 5.37 MeV channels (right panel).

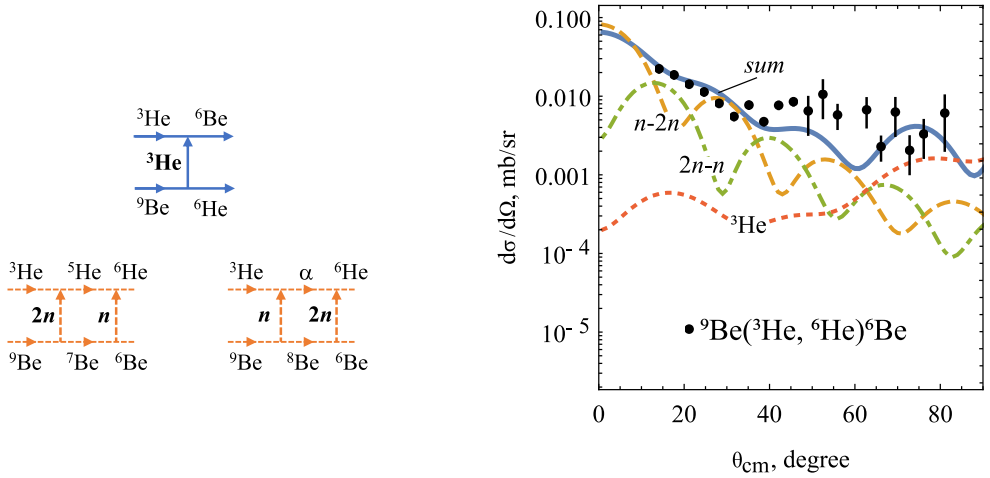

Fig. 9. (color online) Left panel: reaction schemes for one-(solid) and two-step (dashed) transfer mechanisms for ^{9}Be (^{3}He, ^{6}He) ^{6}Be. Right panel: comparison of the CRC differential cross sections with the experimental data for the same reaction.

these mechanisms were calculated within the CRC framework, employing spectroscopic amplitudes and optical potentials without modifications. The primary pick-up of the valence neutron was found to be prominent in the cluster transfer channels, except in those involving ^{6}Li excitations. This observation highlights the cluster structure of n + ^{8}Be in ^{9}Be.

Special interest is drawn to the channel ^{6}He + ^{6}Be. Within the CRC framework, we achieved good congruence between the calculated cross sections and experimental data by proposing two-step transfer mechanisms, *n-2n* and *2n-n*. Nonetheless, the high values of spectroscopic amplitudes used in the CRC calculations suggest the potential involvement of other processes, such as the direct transfer of three neutrons.

The investigation of one-nucleon transfer channels, along with charge exchange reaction channels, is planned as a continuation of the series of studies focusing on the reaction ^{3}He + ^{9}Be at an energy of 30 MeV.

ACKNOWLEDGEMENTS

We would like to thank the Nuclear Physics Institute (NPI) in Řež for providing us with the opportunity to perform this study, as well as the cyclotron staff of the institute for their excellent beam quality.

References

[1] A. Karpov, A. Denikin, M. Naumenko *et al.*, Nucl. Instrum. Meth. Phys. Res. Sect. A **859**, 112 (2017)

[2] C. Lederer and V. Shirley, *Table of Isotopes John Wiley & Sons* (7th edition John Wiley and Sons, New York, USA, 1978)

[3] F. Ajzenberg-Selove , Nucl. Phys. A **490**, 1 (1988)
[4] R. Lichtenthäler, O. Santos, A. Serra *et al*., Eur. Phys. J. A **57**, 1 (2021)
[5] B. S. Huang and Y. G. Ma *et al*, Phys. Rev. C **103**, 054318 (2021)
[6] H. Fortune, Nucl. Phys. A **1014**, 122249 (2021)
[7] V. Starastsin, A. Demyanova, A. Danilov *et al*., Eur. Phys. J. A **57**, 334 (2021)
[8] H. Maridi, A. Pakou, and K. Rusek, Int. J. Mod. Phys. E **30**, 2150024 (2021)
[9] Z. M. Mahmoud and O. S. Qandil, Phys. At. Nucl. **84**, 711 (2021)
[10] A. Amar, Int. J. Mod. Phys. E **31**, 2250011 (2022)
[11] A. Amar and A. A. Ibraheem, Int. J. Mod. Phys. E **30**, 2150090 (2021)
[12] U. Umbelino, K. Pires, R. Lichtenthäler *et al*., Phys. Rev. C **99**, 064617 (2019)
[13] A. Rudchik, E. I. Koshchy, E. A. Budzanowski *et al*., Nucl. Phys. A **609**, 147 (1996)
[14] S. Lukyanov, M. Harakeh, M. Naumenko *et al*., Journal of Physics: Conference Series, **724**, 012031 (2016)
[15] B. Urazbekov, Journal of Physics: Conference Series, **2453**, 012015 (2023)
[16] I. J. Thompson, Comput. Phys. Rep. **7**, 167 (1988)
[17] R. D. Woods and D. S. Saxon, Phys. Rev. **95**, 577 (1954)
[18] Jr. F. Becchetti and G. Greenlees, *Polarization Phenomena in Nuclear Reactions* (*Proceedings* no. 3) (University of Wisconsin Press, 1971)
[19] M. Harakeh, J. Van Popta, A. Saha *et al*., Nucl. Phys. A **344**, 15 (1980)
[20] H. Votava, T. Clegg, E. Ludwig *et al*., Nucl. Phys. A **204**, 529 (1973)
[21] Y. Jiang, J. L. Lou, Y. L. Ye *et al*. (RIBLL Collaboration), Phys. Rev. C **101**, 024601 (2020)
[22] D. Janseitov, S. Lukyanov, K. Mendibayev *et al*., Int. J. Mod. Phys. E **27**, 1850089 (2018)
[23] J. Cook, Nucl. Phys. A **388**, 153 (1982)
[24] D. Kurath and D. Millener, Nucl. Phys. A **238**, 269 (1975)
[25] K. Potthast, H. Brand, H. Freiesleben *et al*., Nucl. Phys. A **614**, 95 (1997)
[26] Y. T. Oganessian, V. Zagrebaev, and J. Vaagen, Phys. Rev. C **60**, 044605 (1999)
[27] D. T. Khoa and W. Von Oertzen, Phys. Lett. B **595**, 193 (2004)